IOP Publishing | Institute of Physics and Engineering in Medicine Physics in Medicine & Biology

Phys. Med. Biol. **60** (2015) 8067–8086 doi:10.1088/0031-9155/60/20/8067

Monte Carlo simulation of prompt γ-ray emission in proton therapy using a specific track length estimator

W El Kanawati[1], J M Létang[1], D Dauvergne[2], M Pinto[2], D Sarrut[1], É Testa[2] and N Freud[1]

[1] CREATIS, Université de Lyon, CNRS UMR5220, Inserm U1044, INSA-Lyon, Université Lyon 1, Centre Léon Bérard, 69007 Lyon, France
[2] IPNL, Université de Lyon, CNRS/IN2P3 UMR5822, Université Lyon 1, 69007 Lyon, France

E-mail: jean.letang@creatis.insa-lyon.fr

Received 28 January 2015, revised 28 May 2015
Accepted for publication 1 September 2015
Published 1 October 2015

Abstract

A Monte Carlo (MC) variance reduction technique is developed for prompt-γ emitters calculations in proton therapy. Prompt-γ emitted through nuclear fragmentation reactions and exiting the patient during proton therapy could play an important role to help monitoring the treatment. However, the estimation of the number and the energy of emitted prompt-γ per primary proton with MC simulations is a slow process. In order to estimate the local distribution of prompt-γ emission in a volume of interest for a given proton beam of the treatment plan, a MC variance reduction technique based on a specific track length estimator (TLE) has been developed. First an elemental database of prompt-γ emission spectra is established in the clinical energy range of incident protons for all elements in the composition of human tissues. This database of the prompt-γ spectra is built offline with high statistics. Regarding the implementation of the prompt-γ TLE MC tally, each proton deposits along its track the expectation of the prompt-γ spectra from the database according to the proton kinetic energy and the local material composition. A detailed statistical study shows that the relative efficiency mainly depends on the geometrical distribution of the track length. Benchmarking of the proposed prompt-γ TLE MC technique with respect to an analogous MC technique is carried out. A large relative efficiency gain is reported, *ca.* 10^5.

Keywords: proton therapy, prompt-gamma imaging, Monte Carlo simulation, track length estimator, variance reduction

(Some figures may appear in colour only in the online journal)

1. Introduction

Online *in vivo* control of the ion range in a patient during proton therapy is a major challenge for Quality Assurance (QA) of treatments. A few years ago, prompt γ-rays were investigated for beam range verification with proton (Min *et al* 2006) and carbon ion beams (Testa *et al* 2008) and prompt-γ imaging emerged as a promising method (Verburg *et al* 2013, Perali *et al* 2014, Roellinghoff *et al* 2014). Since then, several teams in the world have been progressing toward the construction of first clinical prototypes (Kormoll *et al* 2011, Smeets *et al* 2012, Min *et al* 2012, Llosá *et al* 2013, Pinto *et al* 2014, Krimmer *et al* 2015). The imaging concept is usually designed and optimized with the help of Monte Carlo (MC) simulations (Robert *et al* 2013), which have become the gold standard for physical calculations especially for simulations of prompt γ-rays emitted by proton inelastic interactions in complex geometries. It remains hindered by its slow statistical convergence however. An analytic computation method of prompt γ-ray emissions based on the structure of the dose calculation engines in treatment planning system has recently been proposed (Sterpin *et al* 2015). In the domain of low energy photons, the track length estimator (TLE) method is a standard variance reduction technique in voxel-based dose computation in the kerma approximation (Williamson 1987) and is implemented e.g. in several MC codes (DeMarco *et al* 2002, Smans *et al* 2010, Baldacci *et al* 2015). A split exponential variation of the TLE has recently been proposed for MC simulations of small-animal radiation therapy (Smekens *et al* 2014). A track-length based method has also been developed for the calculation of positron emitter distributions in proton therapy (Parodi *et al* 2007), making use of the MC transport code FLUKA to score the proton fluence discriminated in energy. The efficiency improvement it provides with respect to analogous MC simulation is well known with a substantial efficiency gain and no significant loss of accuracy.

The rationale for using prompt γ-rays induced by the inelastic scattering of protons to control the ion range is illustrated in figure 1. The uncertainty in determining the position of the prompt-γ fall-off (e.g. the point at 80% the profile peak-value) when only contributions from proton inelastic processes are considered remains for this PMMA phantom much below 1 mm indeed. The other main contributions to γ-ray emission are coming from the neutron-associated processes, but the longitudinal profile of their distribution is rather flat and does not convey much information in terms of proton range. The impact of neutron-associated events might be larger when considering γ-ray energies above 7 MeV, but the range [4, 5] MeV photons give by far the most interesting contribution for beam range monitoring (Smeets *et al* 2012). It is also worth mentioning that the dose and the γ-ray emission are correlated but cannot be directly compared.

A detailed statistical study of the proposed prompt-γ TLE MC method, some considerations about implementation issues and a benchmarking analysis with an analogous MC method are developed in this paper.

2. Materials and methods

2.1. Prompt-γ TLE

The idea of this TLE-based MC approach is to design a continuous process along the proton track that locally deposits the expected value of the prompt γ-ray emission (induced by proton inelastic scattering) that would have occured if a large number of protons with the same incident energy had followed the same track element. It is therefore particle specific and applied to all protons, whether primary or secondary. Besides, the output of this prompt-γ TLE proton

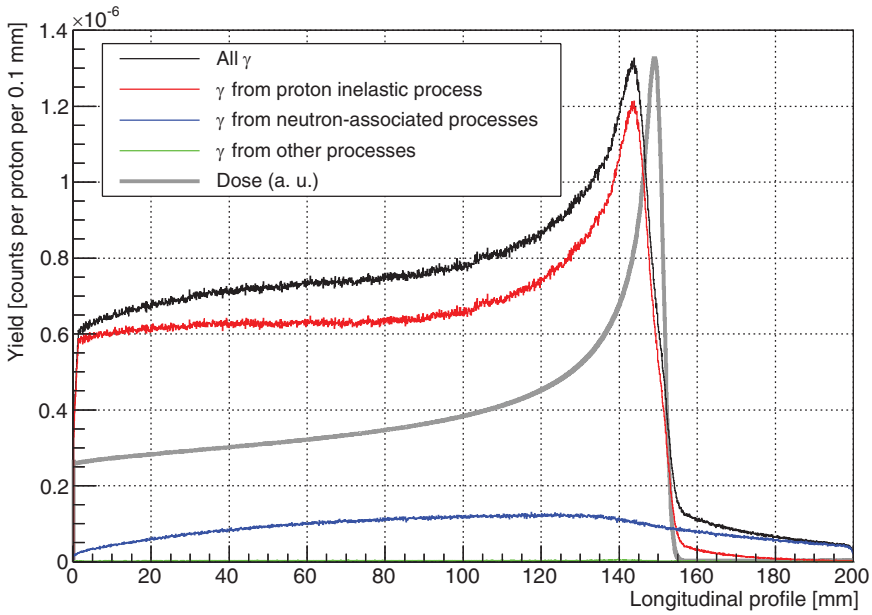

Figure 1. Longitudinal profile of the γ-ray emissions (in the [1–7] MeV energy range) for a 160 MeV proton beam in a homogeneous cylindrical PMMA target (200 mm length and 75 mm radius). All γ-rays were scored at the PMMA target border and selected with a polar angular acceptance in the range [89–91] degrees. Contributions of proton inelastic process (red), neutron-induced processes (blue) and from other processes (green) but they are very few. Geant4 (v10.0.p02) MC simulations with the 'QGSP_BIC_HP' reference physics list. The dose profile (arbitrary unit) is normalized to the maximum of the 'All γ' curve. The projected range of 160 MeV protons is 152 mm in PMMA (from the PSTAR web database (ICRU 1993)).

process is an emission map that is subsequently used to transport those γ-rays in the patient to estimate the dectector response: all resulting secondary photons from electromagnetic processes (Compton scattering, annihilation...) will therefore be taken into account.

We transpose the TLE formalism (Williamson 1987)—originally derived for photon transport problems—to the estimation of the 3D distribution of prompt-γ emitters in proton therapy. Let vector $\boldsymbol{\beta}_{ij} = (r_0(i,j), E_0(i,j), r_1(i,j), E_1(i,j))$ represent the characteristics of the proton corresponding to the ith history and entering its jth linear track at curvilinear abscissa $r_0(i,j)$ and energy $E_0(i,j)$ (so-called 'pre-step' in Geant4 MC simulations (Allison *et al* 2006)), and leaving at curvilinear abscissa $r_1(i,j)$ and energy $E_1(i,j)$ (so-called 'post-step'). An additional scalar $W(i,j)$ can be introduced to represent the proton statistical weight, e.g. to account for additional variance reduction such as MC splitting or Russian roulette. In terms of naming convention, a track will refer throughout this paper to a linear spatial increment along the proton range (it is called 'step' in Geant4 MC code).

Each proton history $\boldsymbol{\alpha}_i$ can be represented by a sequence of linear tracks of the form $\boldsymbol{\alpha}_i = (\boldsymbol{\beta}_{i0}, \boldsymbol{\beta}_{i1}, ...,)$. The problem is to estimate the expectation of the proton prompt-γ spectrum $\boldsymbol{S}(v)$—a vector of the number of prompt γ-rays per energy bin—in a given volume of interest (VOI) v composed of material m_v for any finite collection of histories $\{\boldsymbol{\alpha}_i\}_{i=1}^{n}$. Given an estimator $\boldsymbol{s}(v, \boldsymbol{\beta}_{ij})$ which defines the contribution of each simulated proton track $\boldsymbol{\beta}_{ij}$ to $\boldsymbol{S}(v)$, an estimate $\widehat{\boldsymbol{S}}$ of the prompt-γ spectrum based on n histories can be made:

$$\widehat{\boldsymbol{S}}(v) = \frac{1}{n}\sum_{i=1}^{n}\sum_{j=1}^{t_i}\boldsymbol{s}(v,\boldsymbol{\beta}_{ij}) \tag{1}$$

where subscript i denotes the history $\boldsymbol{\alpha}_i$, subscript j denotes the order of the linear tracks within $\boldsymbol{\alpha}_i$, and t_i is the number of tracks comprised in $\boldsymbol{\alpha}_i$, including incident and secondary protons (created by nuclear collisions). The prompt-γ spectrum estimator $\boldsymbol{s}(v,\boldsymbol{\beta}_{ij})$ is given by

$$\boldsymbol{s}(v,\boldsymbol{\beta}_{ij}) = \int_{r_0(i,j)}^{r_1(i,j)} \delta_v(r)\boldsymbol{\Gamma}_{m_v}(E(r))\mathrm{d}r \tag{2}$$

where

- r stands for the curvilinear abscissa along the proton multi-linear path;
- $\delta_v(r)$ is 1 if the 3D position at the curvilinear abscissa r is in voxel v, and 0 otherwise;
- and $\boldsymbol{\Gamma}_{m_v}(E)$ is the expectation of the linear prompt-γ spectrum in material m of a given volume v for proton energy E, i.e. a vector containing the number of prompt-γ per distance and per prompt-γ energy bin;

In practice, if the track length $|r_1(i,j) - r_0(i,j)|$ is very small (e.g. if the size of the VOI is small and/or an upper bound is used in the MC simulation), the variation in energy of the proton along the track—from $E_0(i,j)$ to $E_1(i,j)$—remains small enough to consider $\boldsymbol{\Gamma}_{m_v}(E)$ constant along the track. In this case, the prompt-γ spectrum estimator $\boldsymbol{s}(v,\boldsymbol{\beta})$ comes down to

$$\boldsymbol{s}(v,\boldsymbol{\beta}_{ij}) = \boldsymbol{\Gamma}_{m_v}(E_0(i,j))\int_{r_0(i,j)}^{r_1(i,j)} \delta_v(r)\mathrm{d}r \tag{3}$$

which exhibits the track length in volume v, i.e. $L(v) = \int_{r_0}^{r_1}\delta_v(r)\mathrm{d}r$. In equation (1), instead of summing over the t_i tracks within a proton history $\boldsymbol{\alpha}_i$, one could sum over the proton energies (of both the primary and secondary particles within $\boldsymbol{\alpha}_i$ history). Let proton energy E be discretized with $g \in \{1,...,G\}$ the energy index: $E_1 = E_{\min}$ and $E_G = E_{\max}$. Using previous assumption made to derive equation (3), the expression of the prompt-γ spectrum TLE becomes

$$\widehat{\boldsymbol{S}}(v) = \frac{1}{n}\sum_{i=1}^{n}\sum_{g=1}^{G}\boldsymbol{\Gamma}_{m_v}(E_g)L_i(E_g,v) = \sum_{g=1}^{G}\boldsymbol{\Gamma}_{m_v}(E_g)\overline{L}_n(E_g,v) \tag{4}$$

where $L_i(E_g,v)$ corresponds to the total track length of protons of energy E_g in volume v within $\boldsymbol{\alpha}_i$ history, and $\overline{L}_n(E_g,v)$ the arithmetic mean of the n values of $L_i(E_g,v)$.

2.2. Prompt-γ TLE variant : integration over the energy loss

The integration over the distance in equation (2) could be translated to an integration over the proton energy as follows

$$\boldsymbol{s}(v,\boldsymbol{\beta}_{ij}) = \int_{E_1(i,j)}^{E_0(i,j)} \delta_v(r)\frac{\boldsymbol{\Gamma}_{m_v}(E)}{S(E)}\mathrm{d}E \tag{5}$$

where $S(E) = -\langle \mathrm{d}E/\mathrm{d}r\rangle$ is the mean rate of total energy loss (or linear stopping power) of the proton (Beringer *et al* 2012). It is worthy of note that equation (2) cannot be directly integrated since the proton energy varies along the track from r_0 to r_1, but equation (5) makes it possible to use numerical methods to carry out the integration process. This prompt-$\boldsymbol{\gamma}$ TLE variant could be seen as a track energy-loss estimator.

2.3. Prompt-γ spectrum database

To benefit from the proposed prompt-γ TLE approach, the material-dependent prompt-γ spectrum database $\mathbf{\Gamma}_{m_v}(E)$ used in equation (2)–(5) must first be built and stored (measured data could also be used). To be more versatile, we propose (i) to express the spectrum database per element (computed in an offline stage) and then (ii) to combine it into materials using the additivity rule (during the online stage). Details about the proposed MC implementation in Gate for both stages are given in section 2.6.

2.3.1. Offline stage. First, a large number n_{offline} of proton histories is simulated for each element of atomic number Z (typ. from $Z = 2$ to 26). The incident proton beam is monochromatic, with an energy larger than the largest proton energy used in proton therapy (e.g. 250 MeV). The volume extent must be sufficiently large so that no proton (both incident and secondary) can escape. When a proton of energy E undergoes a nuclear inelastic collision, the subsequent prompt γ-rays are counted in a spectrum vector $\boldsymbol{N}_\gamma(Z,E)$ together with a variable $N_{\text{inel}}(Z,E)$ scoring the number of proton inelastic nuclear interactions occurring in energy bin E. Then for each proton energy bin E, the corresponding linear prompt-γ spectrum $\mathbf{\Gamma}_Z(E)$ is obtained through a normalization of $\boldsymbol{N}_\gamma(Z,E)$ by $N_{\text{inel}}(Z,E)$ and the element density $\rho(Z)$, and scaled by $\kappa_{\text{inel}}(Z,E)$ the linear material attenuation coefficient related to the proton inelastic nuclear process of element Z at proton energy E. To sum up, for every element of nuclear atomic number Z and for every proton energy E, we compute offline:

$$\frac{\mathbf{\Gamma}_Z(E)}{\rho_Z} = \frac{\boldsymbol{N}_\gamma(Z,E)}{N_{\text{inel}}(Z,E)} \frac{\kappa_{\text{inel}}(Z,E)}{\rho_Z} \tag{6}$$

which gives the expectation of the mass prompt-γ spectrum for element Z and proton energy E. This elemental prompt-γ spectrum database $\mathbf{\Gamma}_Z$ is stored for all Z.

The ratio $\boldsymbol{N}_\gamma/N_{\text{inel}} = \boldsymbol{\eta}_{\gamma/\text{inel}}(Z,E)$ is the prompt-γ yield vector for a given element Z and at a given proton energy E. The total prompt-γ yield per proton inelastic nuclear collision $\eta^{\text{tot}}_{\gamma/\text{inel}}(Z,E)$ is defined as the sum over all energies of the prompt-γ yield vector $\boldsymbol{\eta}_{\gamma/\text{inel}}(Z,E)$. It is constant and around unity (value depending on Z) for proton energies greater than 50 MeV (see figure 4 of the Results section).

2.3.2. Online stage. During the initialization of the MC simulation, the material prompt-γ spectrum database $\mathbf{\Gamma}_{m_v}(E)$ is computed for each material m in the phantom (or patient) volume with the following stoichiometrically-weighted sum (Bragg additivity rule (Bragg and Kleeman 1905))

$$\mathbf{\Gamma}_{m_v}(E) = \rho_{m_v} \sum_{k=1}^{k_{m_v}} \omega_k \frac{\mathbf{\Gamma}_{Z_k}(E)}{\rho_{Z_k}} \tag{7}$$

where ω_k is the fraction by weight of atomic constituent $k \in \{1, ..., k_{m_v}\}$ of material m_v. If the integration is carried out over the energy (see equation (5)), the additional scaling by the stopping power $S(E)$ should be carried out in the offline stage and directly stored in the elemental prompt-γ spectrum database $\mathbf{\Gamma}_Z(E)/\rho_Z$.

2.4. Prompt-γ TLE relative efficiency

The relative efficiency of the prompt-γ TLE MC method with respect to the analogous one is assessed as follows:

$$\epsilon_{\mathrm{TLE/analog}} = \frac{\left\langle t_{\mathrm{analog}} \right\rangle \sigma^2 \left[\widehat{\boldsymbol{S}}_{\mathrm{analog}} \right]}{\left\langle t_{\mathrm{TLE}} \right\rangle \sigma^2 \left[\widehat{\boldsymbol{S}}_{\mathrm{TLE}} \right]} \tag{8}$$

where $\left\langle t_{\mathrm{analog}} \right\rangle$ and $\left\langle t_{\mathrm{TLE}} \right\rangle$ are the expected values of the computation time per primary particle for the prompt-γ TLE and analogous MC methods respectively. The second part of equation (8) is the variance reduction factor, which is an intrinsic characteristic of the method, whereas the first part—the computation time ratio—is implementation and architecture dependent.

In the following paragraphs, we transpose to the distribution of prompt-γ emitters a TLE statistical analysis that was carried out for dose deposition (Baldacci *et al* 2015). We see from equation (4) that the prompt-γ spectrum TLE uncertainty has two components: the first one comes from the material database $\boldsymbol{\Gamma}_{m_v}$, which is fixed and build once in an offline stage, the second component comes from the proton statistics used in the online stage to compute the distribution of track length L_i. The first component thus brings a systematic uncertainty and the second one a statistical uncertainty. For a volume v composed of material m_v and traversed by a mono-energetic proton beam (energy E), the prompt-γ TLE MC variance of a collection of n histories for the prompt-γ energy bin E_γ is as follows (analytic developments are given in appendix A):

$$\sigma^2 \left[\widehat{S}_{\mathrm{TLE},E_\gamma} \right] \approx \Gamma^2_{m_v E_\gamma}(E) \left(\frac{\sigma^2[L(E,v)]}{n} + \frac{\overline{L}^2_n(E,v)}{N_{\gamma,m_v E_\gamma}(E)} \right) \tag{9}$$

with L the track length and the subscript E_γ used to represent the scalar value at the prompt-γ energy bin E_γ for spectral vectors. The relative prompt-γ TLE MC uncertainty can be written as

$$\frac{\sigma \left[\widehat{S}_{\mathrm{TLE},E_\gamma} \right]}{\widehat{S}_{\mathrm{TLE},E_\gamma}} \approx \sqrt{\frac{\sigma^2[L(E,v)]}{n\ \overline{L}^2_n(E,v)} + \frac{1}{N_{\gamma,m_v E_\gamma}(E)}}. \tag{10}$$

The variable $N_{\gamma,m_v E_\gamma}$, which is the number of prompt-γ that was scored offline in the prompt-γ energy bin E_γ to compute the spectrum $\boldsymbol{\Gamma}_{m_v}(E)$ (see equation (6)), can be taken as large as possible so to make the second term in equation (9) (i.e. the systematic uncertainties) negligible with respect to the first term $\sigma^2[L]$ (i.e. the statistical uncertainties). If there are protons of different energies that pass through volume v (see equation (4)), one could just sum the variances in equation (9), assuming independency of the track length with respect to the proton energy. This gives for VOI v

$$\sigma^2 \left[\widehat{S}_{\mathrm{TLE},E_\gamma} \right] \approx \sum_{g=1}^{G} \Gamma^2_{m_v E_\gamma}(E_g) \left(\frac{\sigma^2[L(E_g,v)]}{n} + \frac{\overline{L}^2_n(E_g,v)}{N_{\gamma,m_v E_\gamma}(E_g)} \right) \tag{11}$$

For the analogous MC case, if VOI v is traversed by mono-energetic protons (energy E), the variance is (analytic developments are given in appendix B):

$$\sigma^2 \left[\widehat{S}_{\mathrm{analog},E_\gamma} \right] \approx \frac{1}{n} \Gamma_{m_v E_\gamma}(E)\ \overline{L}_n(E,v) \tag{12}$$

which gives the following expression for the relative prompt-γ analogous MC uncertainty

$$\frac{\sigma \left[\widehat{S}_{\mathrm{analog},E_\gamma} \right]}{\widehat{S}_{\mathrm{analog},E_\gamma}} \approx \sqrt{\frac{1}{n\ \Gamma_{m_v E_\gamma}(E)\ \overline{L}_n(E,v)}} \tag{13}$$

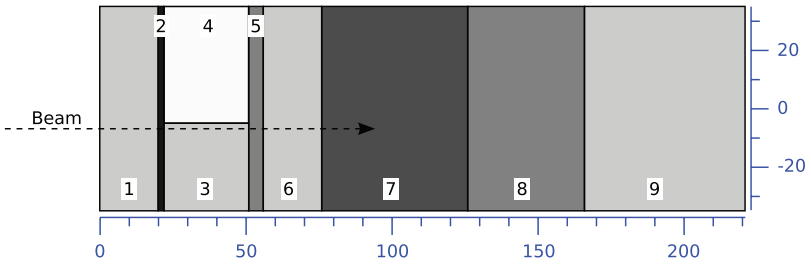

Figure 2. Mid-plane slice of the inhomogeneous phantom (similar to the ones used in Parodi *et al* (2005)). The number labels correspond to material indices in table 1. The phantom is a rectangular parallelepiped (70×70 cm^2 square base and 221 mm length along the beam direction). The proton beam (Gaussian shape with 3.5 mm standard deviation) is shifted 2 mm away from the 4th medium edge (lung equivalent). The rulers in blue are in millimeters.

Equation (12) has to be summed if protons with different incident energy pass through volume v (see equations (4) and (11), the one derived for the TLE case).

The variance reduction factor (for the same number of histories n for both the prompt-γ TLE MC and the analogous one) comes down to

$$\frac{\sigma^2[\,\widehat{S}_{\text{analog},E_\gamma}]}{\sigma^2[\,\widehat{S}_{\text{TLE},E_\gamma}]} \approx \frac{\overline{L}_n(E,v)}{\sigma^2[L(E,v)]}\,\frac{1}{\Gamma_{m_v E_\gamma}(E)} \tag{14}$$

2.5. Phantom and proton source

To evaluate the proposed method, we used a digital phantom consisting of an inhomogeneous target with a rectangular parallelepiped shape, similar to the one that was used in Parodi *et al* (2005) to study the feasibility of in-beam PET for proton therapy monitoring. A sketch of a longitudinal mid-plane slice of the phantom is shown in figure 2. The density and main constituents of each material present in the phantom are listed in table 1.

A monochromatic (160 MeV) proton pencil beam is used with a circular Gaussian-shaped source (3.5 mm standard deviation), a divergence of 2 mrad (standard deviation), and positioned 20 cm away from the phantom. The beam axis is perpendicular to the first material slab and parallel to the Lung-PE interface (2 mm away from it). The projected range, computed from SRIM Ziegler *et al* (2010), is 174.1 mm in water, with a 6.7 mm longitudinal straggling and a 4.3 mm lateral straggling (standard deviations). The last PE slab, i.e. medium 9, intercepts about 2 cm of the range of the protons that pass through the lung-equivalent medium 4 (see figure 2 or 8).

2.6. Monte Carlo implementation and parameters

2.6.1. MC gate 'actors'. Both the analogous MC and the prompt-γ TLE MC have been implemented in Gate 7.0 (using Geant4 10.0 p02) (Allison *et al* 2006, Sarrut *et al* 2014). In the prompt-γ TLE MC case, an 'Actor' has been created in order to generate the elemental prompt-γ spectrum database $\boldsymbol{\Gamma}_Z(E)/\rho_Z$ (see equation (6)), making use of the standard Geant4 function 'GetCrossSectionPerVolume' of a 'G4HadronicProcessStore' instance to estimate $\kappa_{\text{inel}}(Z,E)$. Another 'Actor' has been implemented for the prompt-γ spectrum estimator $\boldsymbol{s}(v,\boldsymbol{\beta})$

Table 1. Mass fractions of the main constituents (from Parodi *et al* (2005)) of the inhomogeneous phantom shown in figure 2.

Medium	ID	H (%)	C (%)	O (%)	Ca (%)	ρ (g·cm^{-3})
PE	1, 3, 6, 9	14.37	85.63	—	—	0.93
PMMA	7	8.05	59.99	31.96	—	1.18
Bone equivalent	2	3.10	31.26	35.57	27.03	1.89
Muscle equivalent	5, 8	8.41	67.97	18.87	2.35	1.00
Lung equivalent	4	8.36	60.41	17.33	—	0.30

Note: PE stands for polyethylene and PMMA for polymethyl methacrylate.

(see equation (3)). In a given VOI v and for a given proton history $\boldsymbol{\alpha}_i$, the prompt-γ TLE spectrum estimator only records the total track length sum $L_i(E, v)$ (see equation (4)) for the proton energy E of a 1D vector (Root TH1D format (Antcheva *et al* 2009)) attached to the VOI. The final prompt-γ spectrum is computed at the end of the simulation for each VOI by a point-wise product between the track-length sum vector and the prompt-γ spectrum database $\boldsymbol{\Gamma}_{m_v}(E)$. All developed Actors will be available in the next Gate version.

2.6.2. Parameters. The recommended 'QGSP_BIC_HP_LIV' physics list was used. An in-depth study of the Geant4 physics lists relevant to prompt-γ imaging in proton therapy can be found in Pinto *et al* (2014). In the analogous MC case, a statistics of 10^7 incident 160 MeV protons has been simulated. In the offline stage, a high statistics—10^9 incident protons at 250 MeV—has been used for each element Z to compute $\boldsymbol{\Gamma}_Z(E)/\rho_Z$ stored as a set of 2D histograms. In the online stage, a lower statistics of 10^4 incident 160 MeV protons has been simulated.

3. Results

3.1. Sampling considerations

In the prompt-γ spectrum database, the proton energy sampling must be fixed with caution since the proton energy determines:

(i) κ_{inel} (in distance^{-1}), the linear attenuation coefficient related to the proton inelastic nuclear process,
(ii) $S(E)$ (in energy · distance^{-1}), the stopping power of the proton, and
(iii) the maximal proton energy loss along the track $\boldsymbol{\beta}_{ij}$ to satisfactorily implement equation (3) or (5).

Figure 3 shows the mass attenuation coefficient $\kappa_{\text{inel}}/\rho$ and figure 4 the total prompt-γ yield $\eta^{\text{tot}}_{\gamma/\text{inel}}$ for bone-, lung- and muscle-equivalent materials (from table 1). Above 30 MeV κ_{inel} varies quite smoothly (below 2% variation per MeV) and $\eta^{\text{tot}}_{\gamma/\text{inel}}$ is almost constant, the proton energy sampling seems not critical to assume constancy of the prompt-γ spectrum within a proton energy bin of 1 MeV. When the proton energy becomes less than 20 MeV, the probability for a proton to undergo an inelastic nuclear process sharply drops and the corresponding CSDA (continuous-slowing-down approximation) range falls below a few millimeters (see figure 5). It is worthy of note in figure 4 that changes in the material composition induce the prompt-γ yield $\eta^{\text{tot}}_{\gamma/\text{inel}}$ to vary significantly. This property could be used with a time and energy resolved prompt-γ detector to monitor the ion range and carry out an elemental analysis at

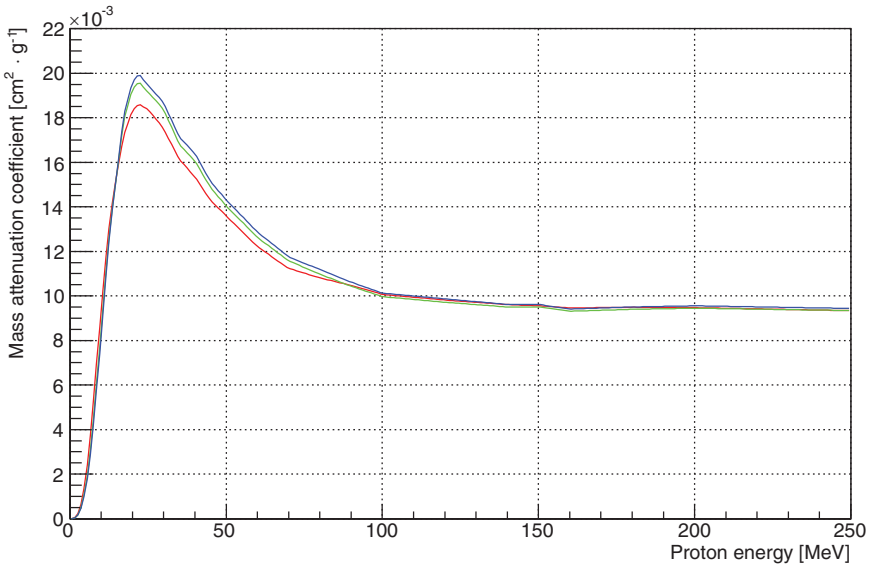

Figure 3. Mass attenuation coefficient of proton inelastic nuclear processes $\kappa_{\text{inel}}/\rho$ (cm^2 g^{-1}) for bone-equivalent (red line), lung-equivalent (green line) and muscle-equivalent (blue line) materials (see table 1). Data from Geant4.10.0.p02 ('QGSP_BIC_HP_LIV' physics list), a comparison of Geant4 models for nucleon-nucleus cross sections with experimental data can be found in Folger and Grichine (2007).

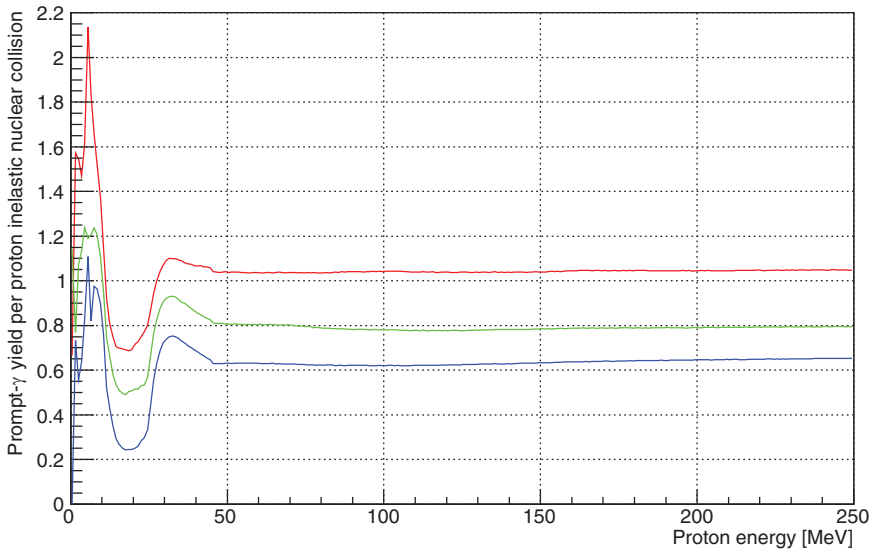

Figure 4. Total prompt-γ yield per proton nuclear inelastic process $\eta^{\text{tot}}_{\gamma/\text{inel}}$ for bone-equivalent (red line), lung-equivalent (green line) and muscle-equivalent (blue line) materials (see table 1) as a function of proton energy. Data from Geant4.10.0.p02 ('QGSP_BIC_HP_LIV' physics list).

the same time (Polf *et al* 2009), but the nuclear reactions of relevance to proton therapy need further theoretical and experimental studies to get a better accuracy (Verburg *et al* 2013). The considerable variations of the prompt-γ yield for low proton energies come from resonant

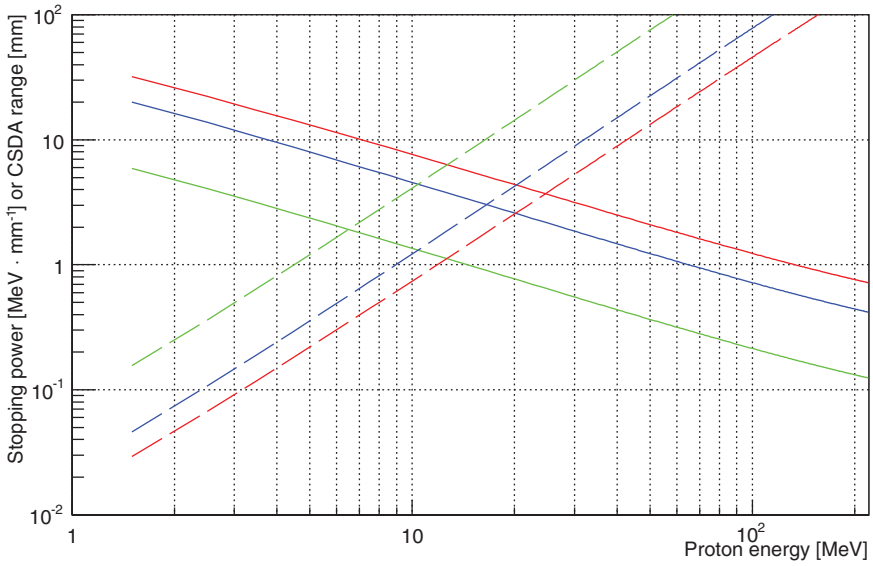

Figure 5. Stopping power $-\mathrm{d}E/\mathrm{d}x$ (solid lines, in MeV·mm^{-1}) and CSDA range (dashed lines, in mm) for bone-equivalent (red line), lung-equivalent (green line) and muscle-equivalent (blue line) materials (see table 1). Data from Geant4.10.0.p02 ('QGSP_BIC_HP_LIV' physics list), which are found in good agreement with the NIST reference data (Amako *et al* 2005).

proton radiative capture processes $A(p,\gamma)B$, whose cross sections have a Breit–Wigner form Breit and Wigner (1936).

The variation in stopping power $S(E)$ with respect to proton energy E is much larger than the variation in $\kappa_{\mathrm{inel}}(E)$ as can be seen in figures 3 and 5. Since $S(E)$ exponentially decreases as the proton energy E increases, the largest variation in $S(E)$ occurs for low energy protons. If a 1 MeV regular binning for the proton energy is used to sample the database $\mathbf{\Gamma}_{m_v}$, there is a variation of about $\pm 4\%$ of stopping power in the energy bin corresponding to a 10 MeV proton.

In order to adequately apply equations (3) or (5), i.e. to avoid having to integrate the spectrum database across different energy bins (making use of equations (2) or (5)), the energy loss of a proton along its track should ideally be smaller than the bin width of the proton energy in the database $\mathbf{\Gamma}_{m_v}$. If the VOI size does not sufficiently bound these proton tracks, a specific track-length limiter should be used in the MC simulation. For example, 10 MeV protons have a stopping power $S(10\ \mathrm{MeV}) = 44\ \mathrm{MeV{\cdot}cm^{-1}}$ in muscle-equivalent material (the corresponding CSDA range is 1.3 mm), which gives a proton track length of 230 μm per 1 MeV proton energy loss (i.e. the bin width of the proton energy): an upper bound of 100 μm (i.e. the maximum distance a proton can travel in a single MC track or step) would be satisfactory in the MC simulation.

3.2. Integration process

To give some insights whether integrating over the proton track length (see equation (3)) is more appropriate or not than integrating over the proton energy loss (see equation (5)), the total number of prompt γ-rays has been plotted in terms of proton energy for the bone-equivalent material in the case of both the prompt-γ spectrum per millimeter and per energy loss (see figure 6). In this figure, the proton energy for which the total number of prompt γ-rays

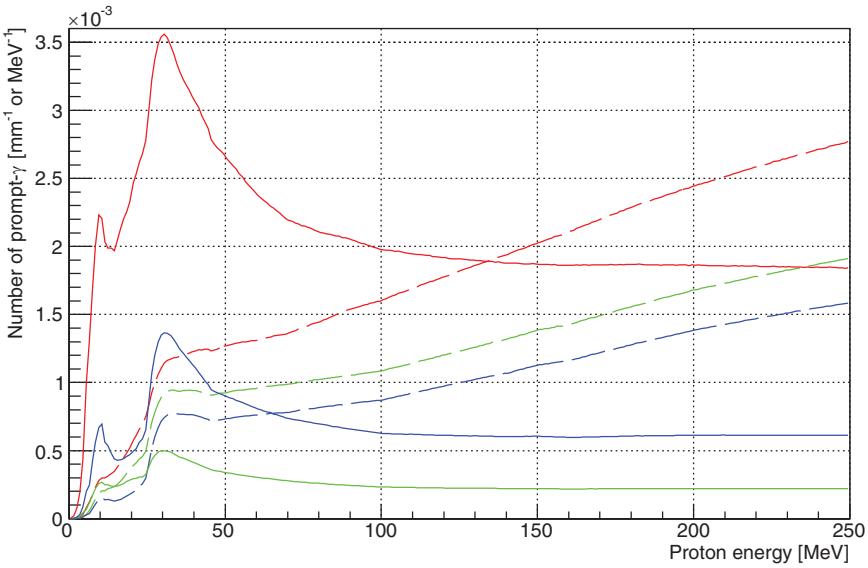

Figure 6. Total number of prompt γ-rays as a function of proton energy in the prompt-γ spectrum per millimeter (solid lines, related to equation (3)) or per proton energy loss (dashed lines, related to equation (5)) for bone-equivalent (red lines), lung-equivalent (green lines) and muscle-equivalent (blue lines) materials from table 1.

expressed per distance or per energy loss are equal corresponds for each material to a stopping power of 1 MeV·mm^{-1} according to figure 5. Both models quite give the same prompt-γ yield.

Equations (3) and (5) have been derived assuming that the prompt-γ spectrum remains constant along a proton track. Figure 6 represents the total number of prompt-γ as a function of the proton energy in both cases. Between 30 and 90 MeV, the total number of prompt-γ per proton energy loss varies much less than the one per millimeter: the assumption of constant prompt-γ spectrum within a proton energy bin in the database is thus more easily validated when integrating over the proton energy loss (i.e. equation (5)). For protons of higher energies however, integrating over the distance (i.e. equation (3)) is more suited because the prompt γ database expressed per distance varies much less than the one expressed per proton energy loss (see figure 6). The relevance of the integration process is not further considered in the paper, and the classical integration over the track length will be used in the following sections.

An example of these 2D histograms simulated for the bone-equivalent material is presented in figure 7. The proton energy is sampled every 1 MeV between 0 and 250 MeV, and the prompt-γ spectrum is sampled every 100 keV between 0 and 8 MeV. For energy below 20 MeV protons, very few proton inelastic nuclear processes occur: the prompt-γ spectrum is composed of just a few γ rays that correspond to the excited states of the atom nuclei. In figure 7, the spectra of the bone-equivalent material clearly exhibits several characteristic discrete γ-rays (Ajzenberg-Selove 1990, Tilley *et al* 1993, Cameron and Singh 2004):

- the 6.129 MeV γ-ray corresponds to ^{16}O$(p,p')^{16}$O* reactions,
- the 4.438 MeV γ-ray corresponds to ^{12}C$(p,p')^{12}$C* reactions,
- the 3.857 and 3.904 MeV γ-rays fall in the same prompt-γ energy bin and correspond to ^{16}O$(p,\gamma)^{17}$F* and ^{40}Ca$(p,p\gamma)^{40}$Ca* reactions respectively.
- the 0.495 MeV γ-ray corresponds to ^{16}O$(p,\gamma)^{17}$F* reactions.

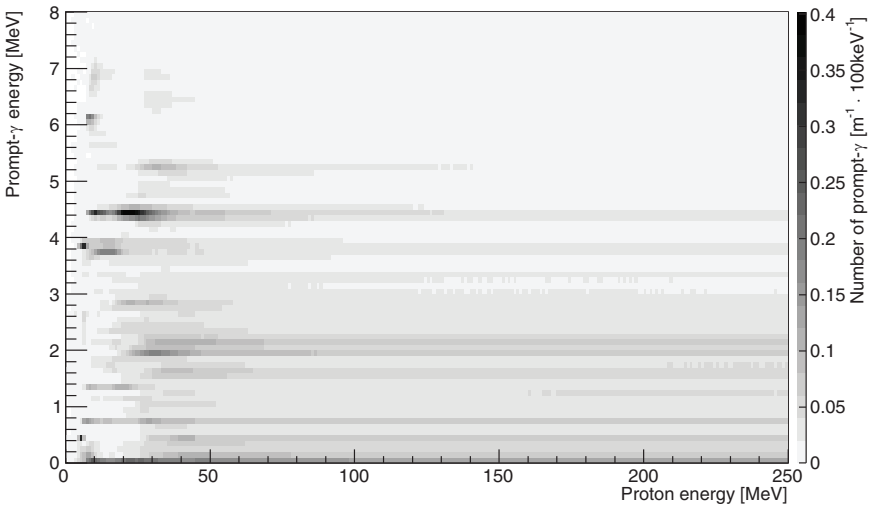

Figure 7. Prompt-γ spectrum $\mathbf{\Gamma}_{m_v}$ for the bone-equivalent material. The unit of the grey-level look-up table is in number of prompt-γ per m and per 100 keV photon energy bin.

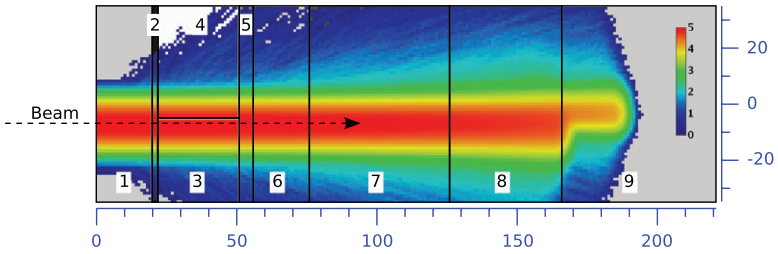

Figure 8. Distribution of the flux of the incident protons per mm^3 in the mid-plane slice of the inhomogeneous phantom corresponding to 10^7 incident protons in the analogous MC. Horizontal and vertical rulers are in millimeters. The color scale is logarithmic and the powers of ten are shown in the color bar.

3.3. Inhomogeneous phantom

The analogous MC simulation for 10^7 protons took 925 times longer than the prompt-γ TLE MC simulation for 10^4 protons. Therefore, using the $\langle x \rangle$ notation to refer to the average value of x, the ratio of the average computation time per incident proton between both methods is

$$\frac{\langle t_{\mathrm{TLE}} \rangle}{\langle t_{\mathrm{analog}} \rangle} = 1.08 \tag{15}$$

which makes the variance ratio a close figure for the relative efficiency of the prompt-γ TLE MC method with respect to the analogous MC one (for the same number of histories).

Figure 8 represents the distribution of the number of incident protons per mm^3 in the mid-plange slice of the inhomogeneous phantom corresponding to the analogous MC simulation with 10^7 protons. The corresponding distribution of the positions of the production of prompt γ-rays per mm^3 in the mid-plane slice is depicted in figure 9.

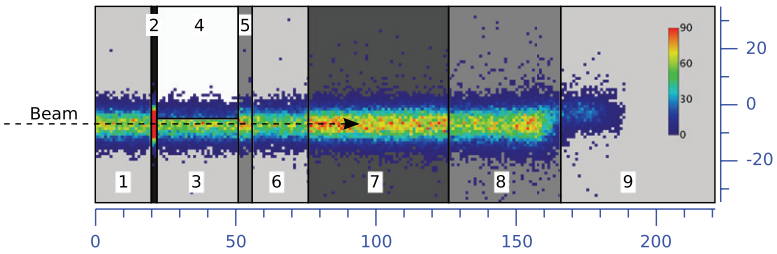

Figure 9. Distribution of the positions of the production of prompt γ-rays per mm^3 in the mid-plane slice of the inhomogeneous phantom corresponding to 10^7 incident protons in the analogous MC. Horizontal and vertical rulers are in millimeters. The value has been clipped to 90 (i.e. higher values are set to 90) for better visualization but only the values in the bone-equivalent slab (medium 2) are affected by it: the true number of prompt-γ in that material is slightly over 200.

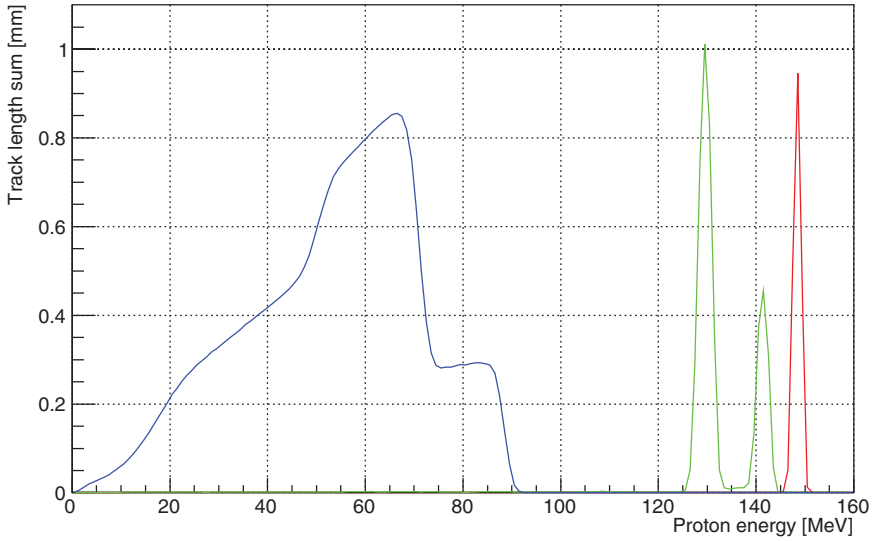

Figure 10. Track length sum per incident proton in medium 2 (red curve), in medium 5 (green curve) and in medium 8 (blue curve). See media in figure 2.

The values of the scored track length vector are shown in figure 10 and are given per incident proton for three different media: the bone-equivalent slab (medium 2), the first muscle-equivalent slab (medium 5) and the second muscle-equivalent slab (medium 8). Prompt-γ spectra for both the analogous and the TLE MC methods are shown in figure 11 for medium 2 (bone equivalent) and medium 8 (muscle equivalent). The 4.4 MeV γ ray is much more visible in the prompt-γ spectrum of medium 8 due to the presence of low energy protons. The difference between the analogous MC and TLE MC prompt-γ spectra divided by the corresponding standard deviation is given in table 2 for medium 2 and for medium 8. The relative uncertainties, both statistical and systematic, are shown in figure 12 for medium 2 and for medium 8.

4. Discussion

The MC computation of the spectrum database during the off-line stage might be quite time consuming if a precision below one percent is required. The systematic uncertainty is directly

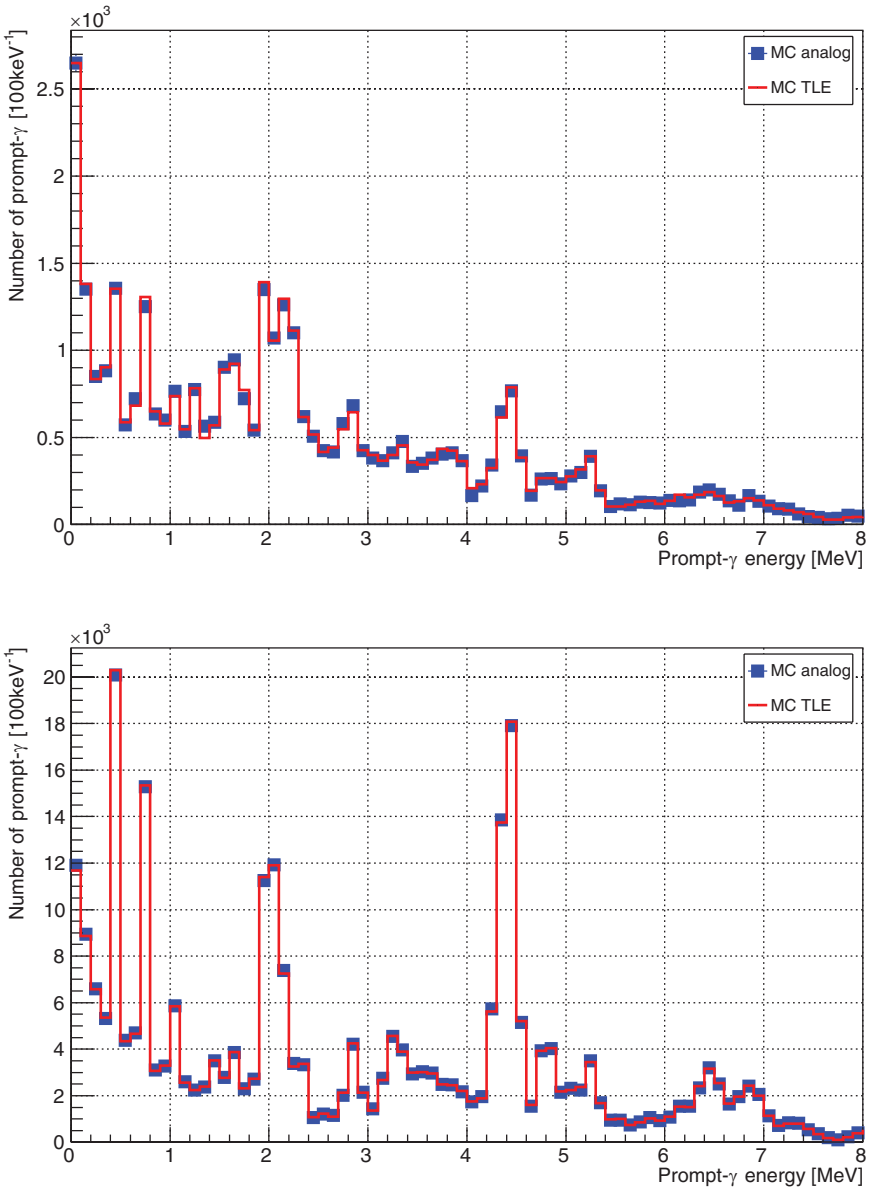

Figure 11. Analogously-derived (10^7 incident protons) versus prompt-γ TLE (10^4 incident protons) spectra. The prompt-γ TLE spectrum is multiplied by 10^3 for better comparison. Top spectra: in medium 2 (bone equivalent). Bottom spectra: in medium 8 (muscle equivalent).

related to the number of incident protons used to build the database and to both the proton and the prompt-γ energy samplings. Relative systematic uncertainties near one percent are expected with energy bins of 100 keV for prompt γ-rays and 1 MeV for incident protons when the spectrum database is build using 10^9 incident protons, which is a rather large number knowing that this process has to be repeated for all elements. If smaller bins, e.g. reduced by a factor of F, were set for the prompt-γ energy bin width, the material prompt-γ spectrum

Table 2. Statistics of the differences divided by the corresponding standard deviations (SD) between the prompt-γ TLE and the analogously-derived prompt-γ spectra.

Medium	2 (bone equivalent)	8 (muscle equivalent)
Average	−0.08	0.10
Standard deviation	1.07	0.99

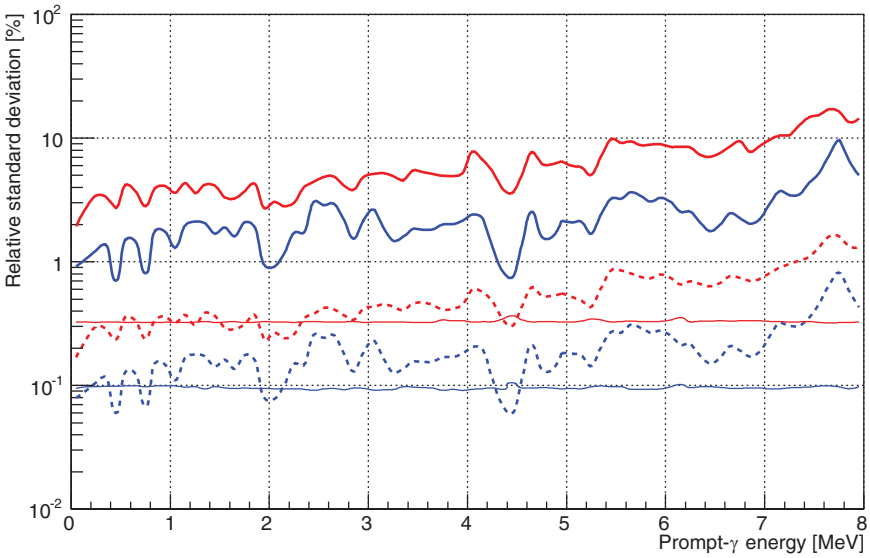

Figure 12. Relative uncertainties. The red curves are for medium 2 (bone equivalent), the blue curves for medium 8 (muscle equivalent). Thick solid lines: relative uncertainty of the analogous MC simulation. Dashed lines: TLE MC systematic relative uncertainty. Thin solid lines: TLE MC statistical relative uncertainty.

database should first be re-built with a statistics F times larger to bring the same systematic uncertainty. During the online stage however, this change of sampling size of the prompt-γ spectrum has very little influence on the performance or the runtime since only the track length is scored by the prompt-γ TLE during the proton MC transportation.

The track length sum in the bone (red curve of figure 10) is very peaked and close to the incident proton energy since the proton beam has only been attenuated by 20 mm of PE (medium 1). The maximum of this distribution is about 1 mm, which is in agreement with the 1 MeV proton energy sampling of the track length vector and the value of the stopping power, which is about 1 MeV·mm^{-1} for 150 MeV protons (see figure 5). In medium 5 (green curve of figure 10), 29 mm downstream of medium 2, two peaks are visible since proton tracks divide between PE and lung-equivalent media before reaching medium 2. The ratio of the first peak with respect to the second is about 0.5. Since the stopping power does not vary much in the 125–140 MeV proton energy range (it varies from 0.6 to 0.56 MeV·mm^{-1}), 130 MeV protons are twice as numerous as those of 140 MeV. Most of the protons pass indeed through PE as we can see in figure 8. The distribution of the blue curve in figure 10 is very broad since incident protons nearly end up their range in that medium.

Looking at the prompt-γ spectra in figure 11, we see that both 4.4 MeV prompt-γ energy peaks do not have the same importance: the Bragg peak region is present in medium 8 (muscle equivalent)—as we can see it in figure 9—while medium 2 (bone equivalent) is only traversed

by high energy protons (see figure 10), medium 2 is likely to exhibit a larger γ-ray continuum and fewer discrete γ-rays. The factor of 20 in prompt γ-rays between these two 4.4 MeV lines—factor whose value could also be inferred from figures 6 and 10—comes from the fact that (i) medium 8 (muscle equivalent) is much larger than medium 2 (bone equivalent) and that (ii) proton energies are much lower in medium 8. In the benchmarking study of the prompt-γ TLE MC method with respect to the analogous one in table 2, the figure-of-merit (FoM) used is the ratio of the difference of the means over the standard deviation (square root of the sum of the variances). The FoM statistics show that both methods are in agreement since the FoM mean is close to 0 (within one standard error of the FoM mean) and the FoM standard deviation close to 1.

The average computation time per incident proton for both MC techniques is comparable: the additional computation time required by the prompt-γ TLE method with respect to the analogous MC is less than 10% since only the proton track length has to be scored at each proton track. At constant number of incident protons, the variance reduction is then a direct figure of the corresponding relative efficiency gain. From the Results section, we can see that the relative efficiency gain of the prompt-γ TLE MC technique to the analogous MC one is very large, around five orders of magnitude: the relative uncertainty of the prompt-γ TLE MC method in figure 12 is about 10 times lower than the analogous MC one while the proton statistics was 10^3 times smaller. We see from equation (14) that the variance reduction factor (VRF) mostly depends on Γ_{m_v} the number of prompt-γ per unit length in the prompt-γ energy bin E_γ, i.e. the VRF is direclty related to the sampling of the prompt-γ energy spectrum in the database.

The variance of the MC prompt-γ TLE method involves two aspects: the uncertainty in the estimation of the local track length distribution (statistical uncertainty) and the statistics used to compute the database (systematic uncertainty). If a too low number of prompt-γ N_γ are scored in the prompt-γ energy bin E_γ to build the database, the prompt-γ TLE MC variance approximation to obtain equation (14) does not hold any longer since $\sigma^2[L]$ might become negligible in equation (9). This would also be the case if the proton beam was parallel to one of the main volume-axes, since the variance of the proton tracks $\sigma^2[L]$ would be close to zero. Therefore, the variance reduction factor would be

$$\frac{\sigma^2\left[\widehat{\boldsymbol{S}}_{\text{analog}}\right]}{\sigma^2\left[\widehat{\boldsymbol{S}}_{\text{TLE}}\right]} \approx \frac{N_{\gamma E_\gamma}(E)}{n\ \Gamma_{m_v E_\gamma}(E)\ \overline{L}_n(E,v)} = \frac{N_{\text{inel}}(E)}{n\ \kappa_{\text{inel}}(E)\ \overline{L}_n(E,v)} \approx \frac{n_{\text{offline}}}{n} \tag{16}$$

which means that the variance reduction factor is in this situation mainly limited by the ratio of statistics used to compute the prompt-γ database and the analogous MC result and is independent with respect to the prompt-γ energy. We can clearly see this statement from figure 12 in which a constant one-decade shift between the systematic TLE and the analogous MC uncertainties is visible. This directly comes from the fact that we used a statistics 100 times greater to compute the database (10^9 incident protons) than to compute the analogous MC output (10^7 incident protons). It is also worthy of note that the statistical uncertainties of the prompt-γ TLE MC method depicted in figure 12 are independent of the proton energy. This is in agreement with the expression of the prompt-γ TLE MC uncertainty given in equation (10).

The number of incident protons in the prompt-γ TLE must be set so as to have a representative distribution of the proton track length in each VOI hit by the proton beam. Inside the green area in figure 8, which covers about ± 3 standard deviations of the beam Gaussian shape, there are more than 10^3 incident proton hits per mm^3. A statistics of 10^4 (i.e. 10^3 times lower than the 10^7 incident protons used to get this figure 8) is a sensible choice for the prompt-γ TLE

method to estimate the distribution of the prompt-γ emitters for the case considered in this study. The necessary statistics for the number of protons per beam in the prompt-γ TLE MC method most likely depends on the beam extent in the transverse plane and on the required 3D spatial resolution.

We can see in figure 12 that both the statistical and systematic uncertainty contributions are of the same level of importance. Knowing *a priori* how large this statistics for the number of protons per beam must be, the balance between both statistical and systematic uncertainties should be preserved for the prompt-γ TLE method to be efficient. In other words, n_{offline}—the number of proton histories in the offline stage to compute the prompt-γ spectrum database—should be set sufficiently large so that both the statistical and the systematic uncertainties have a similar order of magnitude.

As far as the influence of the size of the VOI on the relative efficiency is concerned, equations (10) and (14) exhibit a dependency on the local distribution of the proton tracks in the VOI. Since a value of 0.1 mm has been used to bound the maximum energy loss along a track of the proton range (see section 3.1 on sampling considerations), we should not expect a large dependency on the VOI size: the smaller VOI should have the larger relative statistical uncertainty values though. In figure 12 we indeed see that the relative statistical uncertainty in medium 2 (the thin bone-equivalent slab) is a few times larger than the one on medium 8 (the large muscle-equivalent slab).

5. Conclusions

We have proposed an efficient Monte Carlo variance reduction technique based on the track-length estimator method to compute the distribution of the prompt-γ emitters. A detailed statistical analysis has been reported to characterize the dependency of the variance reduction on the geometrical (track length distribution) and physical (linear prompt-γ spectrum database) parameters. Implementation issues have also been addressed. A relative efficiency of about five orders of magnitude with respect to an analogous MC technique is found. This MC-based technique makes it possible to deal with complex situations such as heterogeneities for which proton straggling and secondary protons may have a decisive contribution. When considering translation to clinic, measurements for the prompt-γ spectrum database, or at least a sound calibration protocol of the simulated prompt-γ spectra, will have to be carried out. The decision-making process on the predicted and observed prompt-γ profiles has also to be finalized for the online monitoring of the proton beam delivery.

Acknowledgments

This work was done in the framework of ENTERVISION FP7-264552, ENVISION FP7-241851, Labex PRIMES ANR-11-LABX-0063, t-Gate ANR-14-CE23-0008, France Hadron ANR-11-INBS-0007 and LYric INCa-DGOS-4664. Simulations have been carried out on the IN2P3 Computing Center.

Appendix A. Prompt-γ TLE MC variance

From equation (4), the variance of the prompt-γ TLE spectrum estimator for the proton energy E can be expressed as a combination of systematic (prompt-γ spectrum database $\mathbf{\Gamma}_{m_v}(E)$) and statistical uncertainties (track length $L(E, v)$) *via*

$$\sigma^2[\,\widehat{S}_{\mathrm{TLE}}] \;=\; \sigma^2[\mathbf{\Gamma}_{m_v}(E)]\,\frac{\sigma^2[L(E,v)]}{n} \;+\; \overline{L}_n^2(E,v)\;\sigma^2[\mathbf{\Gamma}_{m_v}(E)] + \mathbf{\Gamma}_{m_v}^2(E)\,\frac{\sigma^2[L(E,v)]}{n} \tag{A.1}$$

where v is the VOI composed of material m_v. Let us assume material m_v is composed of a single element Z, equation (6) can be generalized for material m_v using equation (7)

$$\mathbf{\Gamma}_{m_v}(E) = \kappa_{\mathrm{inel},m_v}\,\frac{\boldsymbol{N}_{\gamma,m_v}}{N_{\mathrm{inel},m_v}} = \kappa_{\mathrm{inel},m_v}\;\boldsymbol{\eta}_{\gamma/\mathrm{inel},m_v} \tag{A.2}$$

where all variables are function of proton energy E. Let subscript E_γ represent the scalar value at the prompt-γ energy bin E_γ for spectral vectors $\mathbf{\Gamma}_{m_v}$, $\boldsymbol{N}_{\gamma,m_v}$ and $\boldsymbol{\eta}_{\gamma/\mathrm{inel},m_v}$. Using the general error propagation formula, the variance $\sigma^2[\Gamma_{m_vE_\gamma}(E)]$ can be expressed as

$$\begin{aligned}\sigma^2[\Gamma_{m_vE_\gamma}(E)] &= \frac{\kappa_{\mathrm{inel},m_v}^2}{N_{\mathrm{inel},m_v}^2}\,N_{\gamma,m_vE_\gamma} + \frac{N_{\gamma,m_vE_\gamma}^2\,\kappa_{\mathrm{inel},m_v}^2}{N_{\mathrm{inel},m_v}^4}\,N_{\mathrm{inel},m_v} \\ &= \frac{\Gamma_{m_vE_\gamma}^2}{N_{\gamma,m_vE_\gamma}}(1+\eta_{\gamma/\mathrm{inel},m_vE_\gamma}) \approx \frac{\Gamma_{m_vE_\gamma}^2}{N_{\gamma,m_vE_\gamma}}\end{aligned} \tag{A.3}$$

since $\eta_{\gamma/\mathrm{inel},m_vE_\gamma} \ll 1$ if the prompt-γ spectrum is finely sampled (typ. 100 prompt-γ energy bins). Therefore, the variance of the prompt-γ TLE spectrum estimator becomes

$$\sigma^2\,[\,\widehat{S}_{\mathrm{TLE},E_\gamma}] \approx \Gamma_{m_vE_\gamma}^2(E)\left(\frac{\sigma^2[L(E,v)]}{n} + \frac{\overline{L}_n^2(E,v)}{N_{\gamma,m_vE_\gamma}(E)}\right) \tag{A.4}$$

assuming the number of prompt-γ in the material database $N_{\gamma,m_vE_\gamma}(E) \gg 1$.

Appendix B. Prompt-γ analogous MC variance

Transposing the TLE statistical analysis developed in Baldacci *et al* (2015) for dose calculations, the variance of the analogous MC estimator can be expressed in terms of the probability p^*_{analog} of non-zero prompt-γ scoring, which is just an increment of the corresponding prompt-γ energy bin. Therefore, we get for n proton histories

$$\sigma^2\,[\,\widehat{S}_{\mathrm{analog},E_\gamma}] = \frac{1}{n}\,p^*_{\mathrm{analog}}(1-p^*_{\mathrm{analog}}) \tag{B.1}$$

where the probability to have a proton inelastic nuclear collision that gives an prompt-γ in energy bin E_γ is

$$p^*_{\mathrm{analog}} = \left\langle 1-\exp(-\kappa_{\mathrm{inel},m_v}L)\right\rangle \eta_{\gamma/\mathrm{inel},m_vE_\gamma} \tag{B.2}$$

Assuming $\kappa_{\mathrm{inel},m_v}^{-1} \gg L$, the variance of the analogous MC estimator is then

$$\begin{aligned}\sigma^2\,[\,\widehat{S}_{\mathrm{analog},E_\gamma}] &\approx \frac{1}{n}\;\kappa_{\mathrm{inel},m_v}(E)\;\eta_{\gamma/\mathrm{inel},m_vE_\gamma}(E)\;\overline{L}_n(E,v) \\ &\approx \frac{1}{n}\;\Gamma_{m_vE_\gamma}(E)\;\overline{L}_n(E,v)\end{aligned} \tag{B.3}$$

References

Ajzenberg-Selove F 1990 Energy levels of light nuclei A = 11–12 *Nucl. Phys.* **A506** 1–158

Allison J *et al* 2006 Geant4 developments and applications *IEEE Trans. Nucl. Sci.* **53** 270–8

Amako K *et al* 2005 Comparison of Geant4 electromagnetic physics models against the NIST reference data *IEEE Trans. Nucl. Sci.* **52** 910–8

Antcheva I *et al* 2009 ROOT: A C++ framework for petabyte data storage, statistical analysis and visualization *Comput. Phys. Commun.* **180** 2499–512

Baldacci F *et al* 2015 A track length estimator method for dose calculations in low-energy x-ray irradiations: implementation, properties and performance *Z. Med. Phys.* **25** 36–47

Beringer J *et al* 2012 Review of particle physics *Phys. Rev.* D **86** 010001

Bragg W H and Kleeman R 1905 On the α particles of radium, and their loss of range in passing through various atoms and molecules *Phil. Mag. Ser.* **10** 318–40

Breit G and Wigner E 1936 Capture of slow neutrons *Phys. Rev.* **49** 519

Cameron J A and Singh B 2004 Nuclear data sheets for A = 40 *Nucl. Data Sheets* **102** 293–513

DeMarco J J, Wallace R E and Boedeker K 2002 An analysis of MCNP cross-sections and tally methods for low-energy photon emitters *Phys. Med. Biol.* **47** 1321

Folger G and Grichine V 2007 GEANT4 models for nucleon–nucleus cross-sections (NA2 VALSIM) EUDET Memo nr 18

ICRU 1993 Report 49 *Stopping Powers and Ranges for Protons and Alpha Particles* (Bethesda, MD: International Commission on Radiation Units and Measurements)

Kormoll T, Fiedler F, Schöne S, Wüstemann J, Zuber K and Enghardt W 2011 A Compton imager for *in vivo* dosimetry of proton beams: a design study *Nucl. Instrum. Methods Phys. Res.* A **626** 114–9

Krimmer J *et al* 2015 Collimated prompt gamma TOF measurements with multi-slit multi-detector configurations *J. Instrum.* **10** P01011

Llosá G *et al* 2013 First Compton telescope prototype based on continuous $LaBr_3$-SiPM detectors *Nucl. Instrum. Methods Phys. Res.* A **718** 130–3

Min C H, Kim C H, Youn M Y and Kim J W 2006 Prompt gamma measurements for locating the dose falloff region in the proton therapy *Appl. Phys. Lett.* **89** 183517

Min C H, Lee H R, Kim C H and Lee S B 2012 Development of array-type prompt gamma measurement system for *in vivo* range verification in proton therapy *Med. Phys.* **39** 2100–7

Parodi K, Ferrari A, Sommerer F and Paganetti H 2007 Clinical CT-based calculations of dose and positron emitter distributions in proton therapy using the FLUKA Monte Carlo code *Phys. Med. Biol.* **52** 3369–87

Parodi K, Ponisch F and Enghardt W 2005 Experimental study on the feasibility of in-beam PET for accurate monitoring of proton therapy *IEEE Trans. Nucl. Sci.* **52** 778–86

Perali I *et al* 2014 Prompt gamma imaging of proton pencil beams at clinical dose rate *Phys. Med. Biol.* **59** 5849

Pinto M, Dauvergne D, Freud N, Krimmer J, Letang J M, Ray C, Roellinghoff F and Testa E 2014 Design optimisation of a TOF-based collimated camera prototype for online hadrontherapy monitoring *Phys. Med. Biol.* **59** 7653–74

Polf J C, Peterson S, McCleskey M, Roeder B T, Spiridon A, Beddar S and Trache L 2009 Measurement and calculation of characteristic prompt gamma ray spectra emitted during proton irradiation *Phys. Med. Biol.* **54** N519–27

Robert C *et al* 2013 Distributions of secondary particles in proton and carbon-ion therapy: a comparison between GATE/Geant4 and FLUKA Monte Carlo codes *Phys. Med. Biol.* **58** 2879

Roellinghoff F *et al* 2014 Real-time proton beam range monitoring by means of prompt-gamma detection with a collimated camera *Phys. Med. Biol.* **59** 1327–38

Sarrut D *et al* 2014 A review of the use and potential of the GATE Monte Carlo simulation code for radiation therapy and dosimetry applications *Med. Phys.* **41** 064301

Smans K, Zoetelief J, Verbrugge B, Haeck W, Struelens L, Vanhavere F and Bosmans H 2010 Simulation of image detectors in radiology for determination of scatter-to-primary ratios using Monte Carlo radiation transport code MCNP/MCNPX *Med. Phys.* **37** 2082–91

Smeets J *et al* 2012 Prompt gamma imaging with a slit camera for real-time range control in proton therapy *Phys. Med. Biol.* **57** 3371–405

Smekens F, Létang J M, Noblet C, Chiavassa S, Delpon G, Freud N, Rit S and Sarrut D 2014 Split exponential track length estimator for Monte-Carlo simulations of small-animal radiation therapy *Phys. Med. Biol.* **59** 7703–15

Sterpin E, Janssens G, Smeets J, van der Stappen F, Prieels D, Priegnitz M, Perali I and Vynckier S 2015 Analytical computation of prompt gamma ray emission and detection for proton range verification *Phys. Med. Biol.* **60** 4915

Testa E, Bajard M, Chevallier M, Dauvergne D, Le Foulher F, Freud N, Létang J M, Poizat J C, Ray C and Testa M 2008 Monitoring the bragg peak location of 73 MeV u^{-1} carbon ions by means of prompt γ-ray measurements *Appl. Phys. Lett.* **93** 093506

Tilley D, Weller H and Cheves C 1993 Energy levels of light nuclei A = 16–17 *Nucl. Phys.* A **564** 1–183

Verburg J M, Riley K, Bortfeld T and Seco J 2013 Energy- and time-resolved detection of prompt gamma-rays for proton range verification *Phys. Med. Biol.* **58** L37–49

Williamson J F 1987 Monte Carlo evaluation of kerma at a point for photon transport problems *Med. Phys.* **14** 567–76

Ziegler J F, Ziegler M D and Biersack J P 2010 SRIM: the stopping and range of ions in matter (2010) *Nucl. Instrum. Methods Phys. Res.* B **268** 1818–23